Clarifying the charging induced nucleation in glass anode of Li-ion batteries and its enhanced performances

Zhang, Y.F.; Wang, P.X.; Li, G.D.; Fan, J.H.; Gao, Chengwei; Wang, Z.Y.; Yue, Yuanzheng

Published in:
Nano Energy

DOI (link to publication from Publisher):
10.1016/j.nanoen.2018.12.088

Publication date:
2019

Document Version
Accepted author manuscript, peer reviewed version

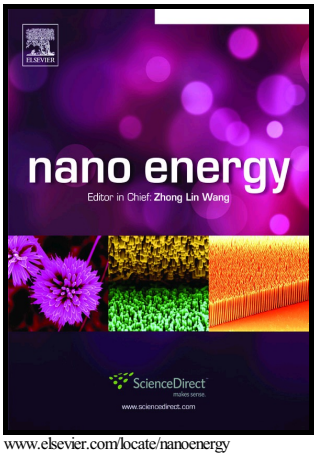

www.elsevier.com/locate/nanoenergy

Clarifying the charging induced nucleation in glass anode of Li-ion batteries and its enhanced performances

Yanfei Zhang, Peixing Wang, Guangda Li, Jiahui Fan, Chengwei Gao, Zhaoyang Wang, Yuanzheng Yue

PII: S2211-2855(18)31001-2
DOI: https://doi.org/10.1016/j.nanoen.2018.12.088
Reference: NANOEN3336

To appear in: *Nano Energy*

Received date: 9 December 2018
Revised date: 27 December 2018
Accepted date: 28 December 2018

Cite this article as: Yanfei Zhang, Peixing Wang, Guangda Li, Jiahui Fan, Chengwei Gao, Zhaoyang Wang and Yuanzheng Yue, Clarifying the charging induced nucleation in glass anode of Li-ion batteries and its enhanced performances, *Nano Energy,* https://doi.org/10.1016/j.nanoen.2018.12.088

Clarifying the charging induced nucleation in glass anode of Li-ion batteries and its enhanced performances

Yanfei Zhang[a1*], Peixing Wang[a,1], Guangda Li[a], Jiahui Fan[a], Chengwei Gao[b], Zhaoyang Wang[c], Yuanzheng Yue[a,b,c*]

[a]School of Materials Science and Engineering, Qilu University of Technology (Shandong Academy of Science), Jinan 250353, China

[b]Department of Chemistry and Bioscience, Aalborg University, 9220 Aalborg, Denmark

[c]State Key Laboratory of Silicate Materials for Architectures, Wuhan University of Technology, Wuhan 430070, China

E-mail: yy@bio.aau.dk (Y.Z.Y.);

zhang-yanfei@hotmail.com (Y.F.Z.)

[*]Corresponding Authors:

Abstract:

It was recently discovered that nanocrystals can be generated in glass anodes by Li-ion insertion, and thereby the cycling stability of Li-ion batteries was enhanced. Here we reveal the origins of both the nanocrystal formation and the enhancement of battery performances by exploring phase transitions, redox reactions, and structural heterogeneity in glass anodes. We infer that Li^+ ions interact with the higher energy domains of structural network during discharging/charging, and some of the Li ions are incorporated into the structural network, and thereby the potential energy is lowered through nanocrystal formation. Upon 5000 discharging/charging cycles at a high current density of 1 A g^{-1}, the nanocrystals in the $40TeO_2$-$60V_2O_5$ glass were identified to be γ-Li_3VO_4. Owing to the metastable nature of the γ-Li_3VO_4 phase, the glass anode becomes electrochemically active and highly ionic conductive. Simultaneously, the cycling stability is greatly enhanced by the nanostructured glass since the nanocrystals could suppress the propagation of micro-cracks generated by volume changes in glass matrix.

[1] These authors contributed equally to this work.

Graphical abstract

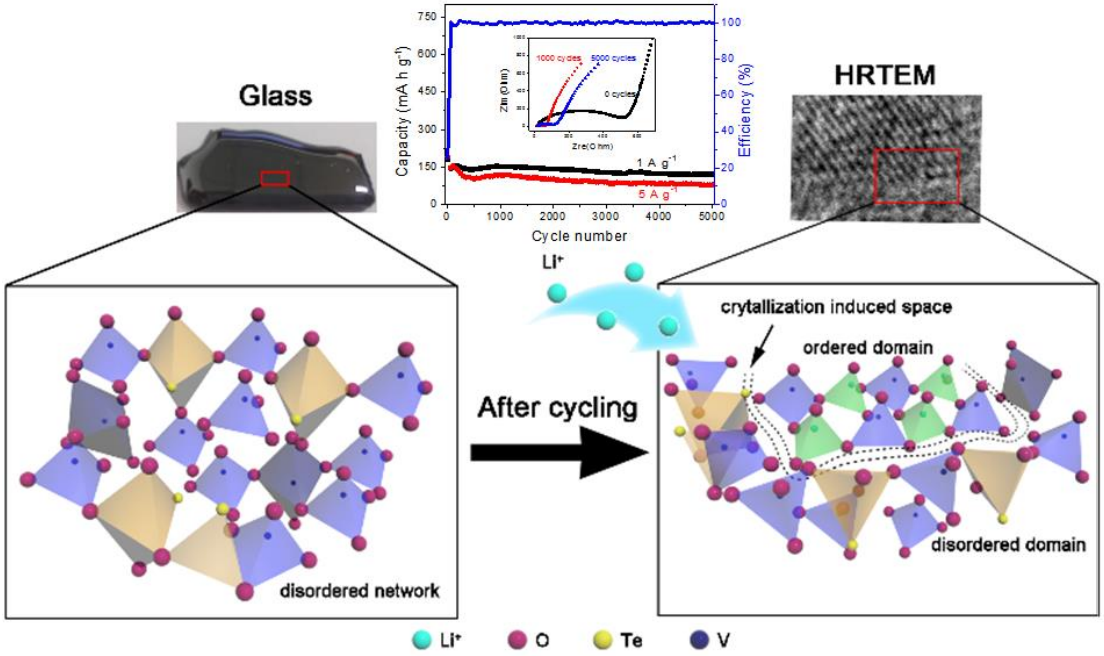

Keywords: Li-ion battery; Anode; Charging induced nucleation; γ-Li_3VO_4 nanocrystal

1. Introduction:

Lithium-ion batteries (LIBs), as one of the most promising energy storage devices, have been applied in many different areas [1-3]. With the ever-growing demand for large-scale energy storage devices and hybrid electric vehicles, it is urgent to develop superior anode materials, which are the main contributor to the battery capacity [4,5], for the next generation of LIBs. To date, most studies of the anode materials have been concentrating on carbonaceous materials [6-8], metal and semi-metal [9-11], as well as metal oxides [12-16]. In all of these materials, the dominant mechanism for Li^+ storage is demonstrated to be the insertion-type lithiation. That is to say, Li^+ ions are inserted into the well-defined layered crystals of the carbonaceous anodes [6-8] or into the interstitial sites of crystalline lattices in metal oxide anodes [2,12,13]. The larger specific capacity of the anode commonly requires an accompanying volume change to accommodate the lithium ions during discharging/charging process. However, the active anode materials suffer from huge volume variations during Li^+ insertion/extraction cycles, leading to pulverization and thus rapid capacity fading.

For instance, silicon is an attractive anode material for lithium batteries since it has a low discharge potential and the highest known theoretical charge capacity (4200 mAh g^{-1}) [17]. However, its large volume expansion (~400%) during lithiation results in fast pulverization of silicon particles and loss of electrical contact between the active material and current collector, and consequently results in rapid capacity fading and short battery lifetime [17].

In contrast to the crystalline anode material, the glass anode as an alternative for rechargeable LIBs has also received attention due to its unique structures, such as absence of grain boundaries, randomly distributed structural units and open network structures [18-22]. During lithiation, Li^+ ions could insert into the structural defects of the amorphous metal oxides [23] or the open network structures of the glass anodes [18-20]. Moreover, the presence of percolation pathways in the glass materials facilitates the diffusion of Li^+ ions, thus leading to superior rate capability [24, 25]. However, the main challenge for employing glass anodes also lies in the rapid capacity decay during discharging/charging processes because of the high polarization and slow diffusion of Li^+ ions and electrons in the active materials although with higher gravimetric and volumetric capacities [19-21]. This severely impedes the practical application of LiBs.

With the above-mentioned aspects in mind, one of the most promising solutions to avoid rapid capacity decay, i.e., to prolong the cycling life, is to combine the advantages of nano-crystals with those of glass materials by designing hierarchical nanostructures [16,18,26-28]. The glass phase plays beneficial roles in different manners. First, the glass phase can effectively buffer the strain/stress induced by volume variations of the crystal phases during the discharging/charging cycles [16]. On the other hand, the glass phase allows the charging-induced crystal growth within nano-scale [18]. As is known, the smaller the crystals in the electrode materials are, the larger the crystal-glass boundary area is, and hence, the easier the Li^+ ions diffuse, leading to better electrochemical performances [29,30]. Second, some oxide glasses containing transition-metal ions, e.g., V ions, exhibit semiconducting behavior that

increases the electrical conductivity of the overall electrodes [24,25]. According to a recent study [31], the V_2O_5 nanowire-reduced graphene oxide (rGO) composite paper could be used as cathode materials for lithium-vanadium batteries. Such cathode materials exhibited excellent electrochemical performances, which were mainly attributed to the integration of the electronic conductivity of rGO with the interconnected networks of both the V_2O_5 nanowires and the solid electrolyte. The amorphous carbon coated Li_3VO_4 has been reported to significantly improve the electrochemical performance of the anodes since the grain growth was strongly restricted by the amorphous carbon layer [27]. However, the negative effects, such as low tap density and large irreversible capacity loss [32], could emerge when using the surface-coating nanostructured materials as electrodes.

Recently, we proposed the disorder/order engineering concept to improve the anode performances. Specifically, we first fabricate the semiconducting V_2O_5-TeO_2 (VT) glass by melt-quenching, then mixed its powder with carbon black and sodium carboxy methyl cellulose to form anode, and finally subjected them to Li ion discharging/charging. After a certain number of cycles, the glass phase was partially transformed into ordered phases at the nanoscale, i.e., nanocrystals, leading to the improved anode performances, in particular, the cycling stability [18]. It should be stressed that the formation mechanism of the nanocrystal is fundamentally different from that of the classical thermally induced crystallization [33,34]. Here the questions arise: what type of crystal emerges during discharging/charging? Why can the crystal phase enhance the electrochemical performance of the VT glass anode? What is the microscopic mechanism of the discharging/charging induced nucleation? In this study, we answered these questions by taking the $60V_2O_5$-$40TeO_2$ (VT60) glass anode as an example. The present study gives insight into the relation between crystal formation and electrochemical performances of the glass anodes for LiBs, as well as into the charging induced crystallization.

2. Experimental section

2.1 Preparation of glass

We chose and prepared the **$60V_2O_5$-$40TeO_2$ (VT60)** glass as anode material by using the conventional melt-quenching method [18]. The relatively low melting temperature (>1073 K) and short melting duration (30 min) were beneficial to minimizing the evaporation of V_2O_5 and TeO_2. The melt-quenched glass was annealed at the glass transition temperature (T_g) for 2 hours, and then cooled naturally down to room temperature to remove the thermal stress.

2.2 Characterization

X-ray diffraction (XRD) patterns of the studied samples were acquired by an X-ray diffractometer (XRD) (Shimadzu LabX XRD-6100, CuKα radiation) from 10º to 70º (2θ) with a stepsize of 0.02. To obtain the XRD patterns of the cycled glass anodes, the test cells were carefully disassembled in an argon-filled glovebox, and the anodes were scraped off. The particle size and morphology of the glass powder before assembling cells were examined by a field emission scanning electron microscope (FE-SEM, ZEISS GeminiSEM500). To detect the microstructural changes of the anodes subjected to long cycles, a high-resolution transmission electron microscope (HRTEM, JEM 2100, accelerating voltage: 200 kV) was employed. The enthalpy relaxation of the fast-quenched VT60 glass was analyzed using a differential scanning calorimeter (DSC) (Netszch Jupiter STA 449F3, Selb, Germany) at the upscan rate of 10 K/min equal to the prior downscan rate in nitrogen, from which the energetic and structural heterogeneity was determined [35]. The valence state of the VT60 glass anode was studied by X-ray photoelectron spectroscopy (XPS, ESCALAB 250Xi) using a focused monochromatized Al Ka radiation ($h\nu$=1486.6eV).

2.3. Electrochemical measurements

The electrochemical properties of VT60 glass anode were evaluated with two-electrode coin cell by an automatic Land battery test system (CT2001A). The working anodes were prepared using the same procedure as described in [18]. The galvanostatic discharging/charging cycling test of the samples was conducted between

0.01 and 3.0 V vs. Li/Li^+ under a high current density of 1 and 5 A g^{-1}, respectively, on a Land battery test system. Cyclic voltammetry (CV) measurements were carried out by using an electrochemical workstation (CHI 660E) at a scan rate of 0.1 mV s^{-1} in the voltage range of 0.01-3.0 V (vs Li/Li^+). Electrochemical impedance spectroscopy (EIS) measurements were conducted on the impedance-measuring unit (PARSTAT 2263 electrochemical workstation) with AC signal amplitude of 10 mV in the frequency range of 100 kHz to 0.01 Hz. All the electrochemical measurements were carried out at the room temperature.

3. Results

The electrochemical performances of the VT60 glass anode in LiBs were evaluated by half-cells. Fig. 1a shows the first three cycles of galvanostatic discharging/charging curves at a current density of 1 A g^{-1}. The initial discharging/charging capacity is found to be 629/196 mA h g^{-1}, resulting in an irreversible capacity retention of 31%. The high capacity loss could be, on one hand, due to the formation of the solid electrolyte interface (SEI) film that lowers the ionic conductivity. On the other hand, the capacity loss could be caused by the disorder-order transition. From our previous findings [18], the Li-containing nano-crystals already appear in the VT60 glass anode during the first discharging/charging cycles. This process could consume a certain amount of Li ions, which were inserted into the glass network and subsequently participated in the resulting nanocrystal structure during the first discharging cycle, leading to a lower initial charging capacity. The efficiency is rapidly increased to 92.8% and 94.3% over the subsequent second and third cycles, corresponding to a stable capacity of about 200 mA h g^{-1}.

Cyclic voltammetry (CV) measurements were also performed and the corresponding first three cycles of the CV curves at a scan rate of 0.1 mV s^{-1} in the voltage range of 0.01~3 V were shown in Fig. 1b. Only a single couple of peaks can be observed, implying the simplified step of Li insertion. The 1st cycle is apparently different from the subsequent two cycles with a small peak at around 0.65 V near the

main reduction peak at 0.58 V. This could be ascribed to the side reaction on the electrode surfaces and to the formation of SEI film. For the subsequent cycles, the reduction peak was found to shift to 0.85 V, indicating a phase transformation accompanied by the reduction of vanadium ions during Li insertion. In addition, a broad oxidation bump at around 1.3 V in all cycles was observed, implying the lithium extraction mechanism related to the oxidation of vanadium ions, and the high reversibility.

Fig. 1c exhibits the long-life performance of the glass anode and the Coulombic efficiency (CE) of about 100%. The capacity can be maintained at 121 mA h g^{-1} at a current density of 1 A g^{-1} after 5000 cycles, with an outstanding capacity retention of 83.7%. The CE of almost 100% has been obtained, indicating the excellent cycling stability of the VT60 glass. At a higher current density of 5 A g^{-1}, the capacity of 80 mA h g^{-1} can be retained after 5000 cycles, corresponding to 53.6% retention of the original capacity.

EIS measurements are carried out to illustrate the electrode kinetics of the VT60 glass anode before and after 1000 and 5000 discharging/charging cycles, respectively. Each EIS spectrum in Fig. 1d exhibits one semicircle in the high frequency region and an inclined line in the low frequency region. The diameter of the semicircle is a measure of the SEI resistance and the charge-transfer resistance. The inclined line is assigned to the Warburg impedance, which is associated with the coefficient of Li^+ ion diffusion into the bulk electrode. As shown in Fig. 1d, and also according to our previous findings [18], the resistance of VT60 glass was greatly reduced after 1000 cycles due to the formation of nanocrystals randomly distributed in the glass matrix. It is clearly seen that the diameter of the semicircle of the VT60 glass after 5000 cycles was slightly larger than that after 1000 cycles, this could be due to some side reactions with the electrolyte, which took place upon super long cycles. Nevertheless, the resistance is still much lower than that of the VT60 glass anode before cycles. To clarify the reasons for the outstanding cycling performance, both the XRD patterns and HRTEM micrographs of the VT60 glass anode after 5000 cycles at 1 A g^{-1} were

taken.

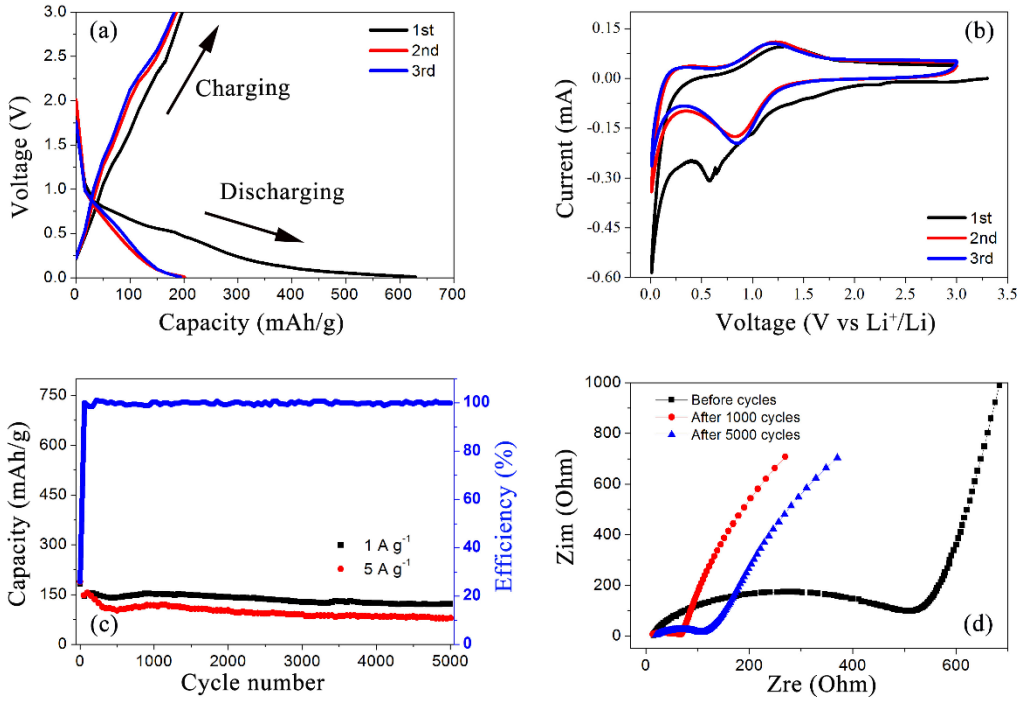

Fig. 1. (a) Galvanostatic discharge and charge curves at 1 A g^{-1}, (b) Cyclic voltammetry curves and (c) Cycling performances of VT60 glass anode at high current densities of 1 and 5 A g^{-1}, respectively. (d) Nyquist plots for VT60 glass anode before and after 1000 and 5000 cycles.

Fig. 2a shows the SEM image of the VT60 glass sample after ball milling for 4 hours at the rotation speed of 400 rpm/min, before cell assembling. It can be seen that the sample is composed of particles with a broad size distribution from dozens of nm to several μm, the average size of which is about 100-200 nm. These particles show smooth surface and irregular shapes. Fig. 2b shows the XRD patterns of both the fresh VT60 glass (black line) and the VT60 glass anode subjected to 1000 and 5000 discharging/charging cycles (red and blue lines) at a current density of 1 A g^{-1}, respectively, as well as the γ-Li_3VO_4 crystals for comparison. The broad hump in the pattern of the fresh VT60 confirms its pure glass nature. According to our previous studies, the nanocrystal phase formed after 1000 cycles was identified to be $LiVO_3$, which is an unstable crystal phase [18,36]. With increasing discharging/charging cycles up to 5000, the characteristic peaks of the γ-Li_3VO_4 phase (JCPDS Card no.: 24-0666) gradually appear besides some minor peaks attributed to $LiVO_3$.

Furthermore, the intensities of γ-Li_3VO_4 diffraction peaks are much higher than those of $LiVO_3$, implying that γ-Li_3VO_4 is the predominant crystalline phase in the glass anodes after 5000 cycles. In addition, both γ-Li_3VO_4 and $LiVO_3$ crystals are intercalation materials, which can give electrodes superior electrochemical performances [2,37]. X-ray photoelectron spectroscopy (XPS) was measured to study the valence state variation of vanadium ions for the VT60 glass anode before and after 5000 cycles at 1 A g^{-1}. For the fresh VT60 glass (Fig. 2c), four peaks at 514.9, 521.7, 516.4 and 523.9 eV can be assigned to the $2p_{3/2}$ and $2p_{1/2}$ for V^{4+}, $2p_{3/2}$ and $2p_{1/2}$ for V^{5+}, respectively [38]. The molar ratio of the V^{4+} to V^{5+} ions in fresh VT60 glass was determined to be about 0.06. The presence of V^{4+} in the fresh VT60 glass could be attributed to the equilibrium redox reaction during glass melting in atmospheric air. It is generally established that the higher the melting temperature is, the more favorable are the lower valence states of transitional metals. After 5000 discharging/charging cycles, it can be seen that two dominant peaks are observed at 517 and 524.2 eV (Fig. 2d), matching with the $2p_{3/2}$ and $2p_{1/2}$ spin-orbit levels of V^{5+}, respectively, implying that nearly all the V^{4+} ions were oxidized to the V^{5+} ions upon 5000 discharging/charging cycles.

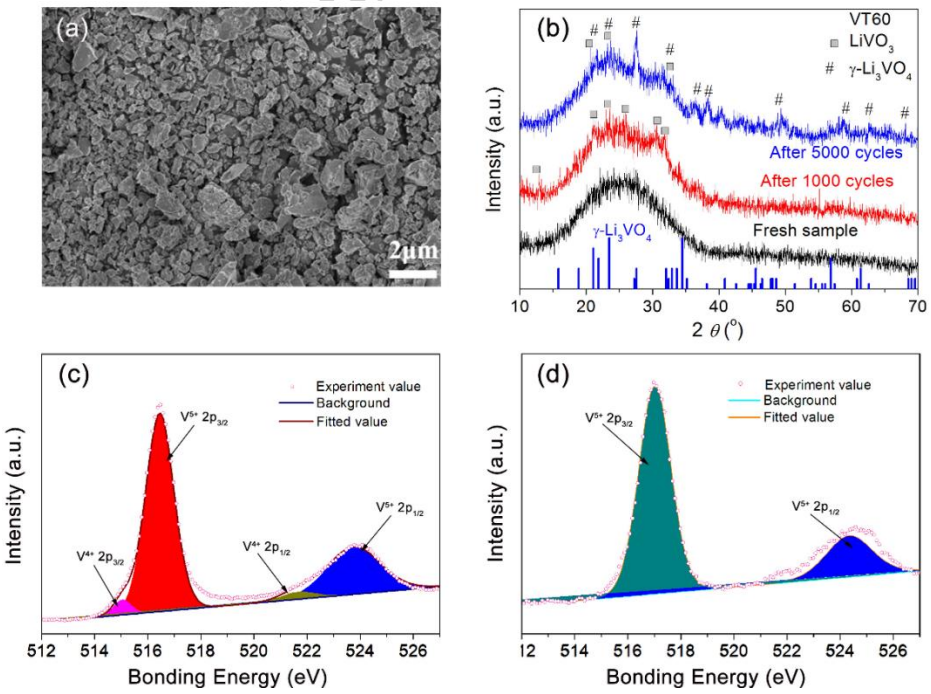

Fig. 2. (a) SEM image of the VT60 glass particles after ball milling. (b) The XRD analysis of the fresh (ball milled) VT60 glass, the VT60 glass anode after 1000 and 5000 discharging/charging cycles at a current density of 1 A g^{-1} and the γ phase Li_3VO_4 crystal. (c) and (d) V 2p X-ray photoelectron (XPS) spectrum of VT60 glass before and after 5000 discharging/charging cycles at 1 A g^{-1}.

Fig. 3 shows the high-resolution TEM (HRTEM) images of the VT60 glass anode after 5000 cycles at the current density of 1A g^{-1}, where it is seen that the microstructure of the sample significantly differs from the amorphous structure of the fresh glass (i.e., before cycling) [18]. As shown in Figs. 3a and b, a large number of structurally ordered domains at nanoscale (represented by dark domains) with a mean size of about 10 nm and clear boundaries are randomly distributed in the glass matrix, forming the nano-glass ceramic structure. These nanocrystals are isolated from each other. Fig. 3c shows the legible ordered lattice fringes with different basal distances. The crystal interplanar spacing of 0.2 nm, 0.235 nm and 0.33 nm correspond to the (320), (112) and (121) planes of γ-Li_3VO_4 (JCPDS Card no.: 24-0666), respectively. In addition, the amorphous matrix, in which the ordered lattice fringes are embedded, can also be clearly observed. This type of nanostructured glass is verified by the XRD result (Fig. 2b). Fig. 3d shows the selected area electron diffraction (SAED) pattern for the denoted area in Fig. 3c. The circular diffraction spots in SAED pattern demonstrate the nanocrystalline phase from VT60 glass anode after 5000 cycles. This implies that the electrochemical activation, i.e., the lithiation/delithiation process, can lead to the morphology variation by formation of a large number of nanocrystals from the glass matrix. The nanostructured glass (i.e., nano glass-ceramics [26]) could facilitate the electrochemical reactions between electrode and electrolyte and improve the structure stability of the VT60 glass anode, resulting in superior electrochemical performances, especially cycling stability.

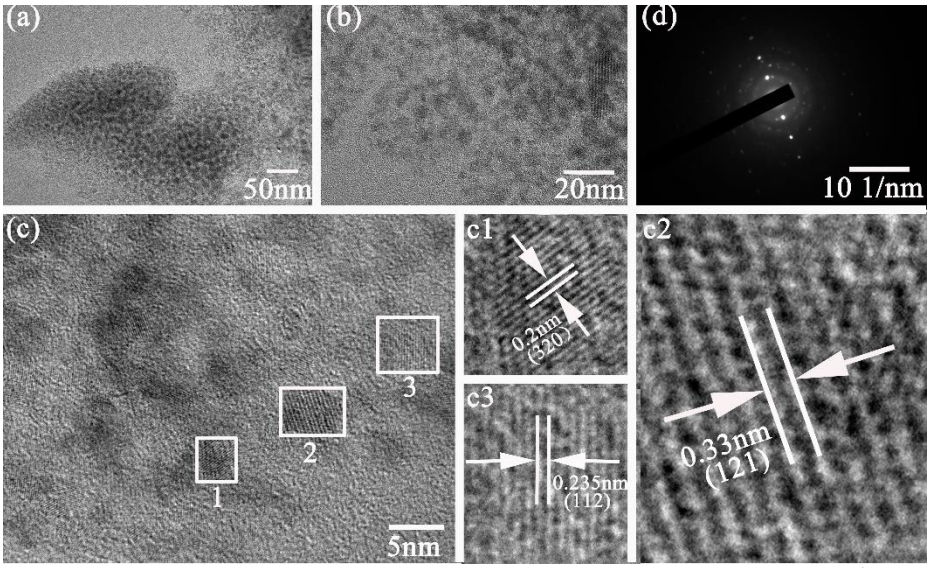

Fig. 3 HRTEM images (a), (b) and (c) of the VT60 glass anodes after 5000 discharging/charging cycles at the current density of 1 A g^{-1}. c1, c2 and c3: the enlarged images of the regions denoted in (c), respectively, illustrating the interplanar spacing. (d): corresponding SAED pattern of the crystallized area in (c).

4. Discussions

To investigate the cycling stability of VT60 glass, we conducted the differential scanning calorimetry (DSC) upscan on the as-produced glass at 10 K/min to 700 K in nitrogen. Fig. 4a shows the DSC curve of VT60 glass with three characteristic temperatures: the onset glass transition temperature (T_g), onset crystallization temperature (T_c) and melting point (T_m), which are 513 K, 554 and 820 K, respectively [39]. The glass stability against crystallization was found to have a parallel relation to the glass forming ability [40,41], and the former can be described by the Hruby parameter, $K_H=(T_c-T_g)/(T_m-T_c)$ [42]. The K_H value of VT60 glass was determined to be only 0.15, implying a rather low glass stability of the studied glass [43]. The low glass stability means the stronger tendency to nucleation and crystal formation due to the presence of the pre-ordered domains at nanoscale in the supercooled liquid state [35,44].

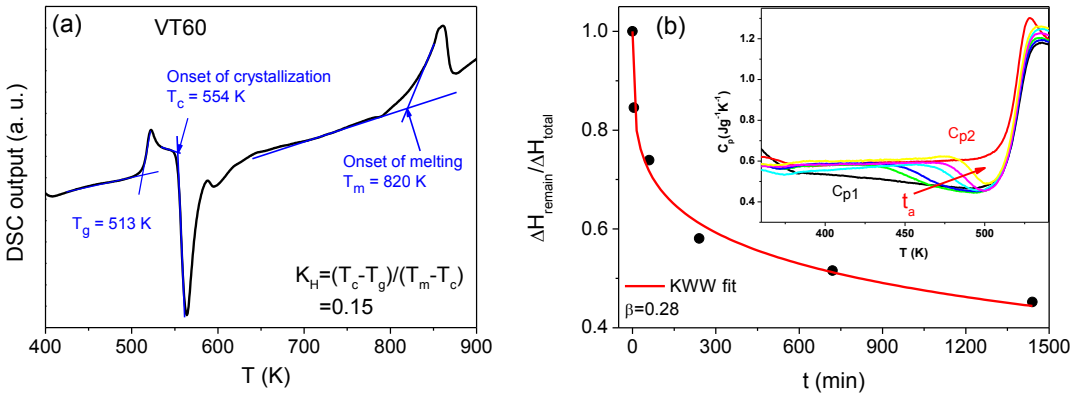

Fig. 4 (a) DSC curve of VT60 glass during heating. The determination of the three characteristic temperatures T_g, T_c and T_m is illustrated. (b)Annealing time (t) dependence of the normalized remaining excess enthalpy ($\Delta H_{remain}/\Delta H_{total}$) in the FQVT60 glass annealed at $0.8T_g$ (410 K), where ΔH_{remain} and ΔH_{total} are the remaining excess enthalpy and the total excess enthalpy, respectively, determined by the C_p curves as shown in the inset.

In terms of the potential energy landscape [45], glass is structurally heterogeneous, i.e., the structure can be described by the spatial correlations of potential energies of structural units [46], i.e., energetic heterogeneity. The structural heterogeneity has a strong impact on the glass properties. The study of structural heterogeneity in both the glassy and the supercooled liquid states is critical for understanding of the nature of glass [47] and how it affects the glass properties [48,49]. The quenching-annealing-DSC approach has been demonstrated to be a powerful tool for detecting the structural heterogeneity in the glassy state [50,51]. The width of the structural relaxation time distribution expressed by the Kohlrausch stretching parameter β can be used as a measure of the extent of the structural heterogeneity [51].

To quantify the structural heterogeneity in the studied VT60 glass anodes, we investigated the enthalpy relaxation of the fast quenched (FQ) VT60 glass, which is prepared by pouring the glass melt into ice water to trap the high potential energy of the supercooled liquid to form a glass state with a higher fictive temperature (T_f) compared to a glass cooled at 10 K/min [51]. Fig. 4b shows the time dependence of the normalized remaining enthalpy in the FQVT60 glass annealed at $0.8T_g$ (410 K). The enthalpy relaxation curves are fitted by the Kohlrausch-William-Watts (KWW) function, i.e., $\Delta H_{remain}/\Delta H_{total} = \exp[-(t/\tau)^{\beta}]$, where β is determined to be 0.28,

indicating a higher degree of structural heterogeneity. From another perspective, the variation of the C_p patterns of the annealed samples with annealing time (inset of Fig. 4b) indicates the dynamically fragile nature of the VT60 composition and a high degree of structural heterogeneity [52,53]. This implies that the fast quenched VT60 glass has a wide distribution of independent micro-domains with different potential energies. Since the cooling rate of the fast quenched VT60 glass is higher than that of the naturally cooled VT60 glass [54], the structural heterogeneity at a higher T_f can be arrested at a lower T_f. In other words, owing to the energetic frustration effect [55,56] upon the glass transition during cooling, the structural domains with different potential energies are frozen in.

During the discharging/charging process, Li^+ ions gradually insert and diffuse into the VT60 glass anode through the electrolyte. Considering the high structural and energetic heterogeneity of the VT60 glass, the structural domains with higher potential energy are vulnerable to Li^+ ions. When these domains with higher energy are hit by the Li^+ ions during insertion, some of these ions will participate in the lattice of the high-energy domains in the glass network, and thereby lower their potential energy by forming ordered structures at nanoscale. As these domains with higher potential energy are randomly distributed in the glass matrix, the formed nanocrystalline domains are also randomly distributed as seen in the HRTEM images (Figs. 3a and b). Furthermore, the firstly formed ordered structural domains can act as the lattice platforms or nucleation sites, to which the Li^+ ions can further diffuse during the subsequent discharging/charging cycles. This leads to the formation of the final nanocrystals upon 5000 charging cycles as we see in Fig. 3.

In addition, the formed ordered structural domains caused by intercalation of Li^+ ions may induce extensive stress in the boundaries between crystals and glass matrix due to volume contraction that is known from the diffusionless crystal growth mechanism [57]. Fig. 5 shows a schematic representation for the structural evolution of VT60 glass anodes upon 5000 discharging/charging cycles. It is seen that, upon intercalation of the Li^+ ions, the disordered network structure is transformed into the

mixed network consisting of both ordered and disordered domains. The volume contraction of the ordered domains due to crystallization could generate more free space (see the channel in the right frame of Fig. 5), particularly in the boundaries between nanocrystals and their surrounded glass matrix, for Li^+ ions to migrate. The excessive space would enhance the transfer kinetics of the Li ions, leading to higher ionic conductivity of the anodes. Moreover, the increased mobility of all the ionic species is beneficial to further local structural rearrangement, and hence, to nanocrystal formation.

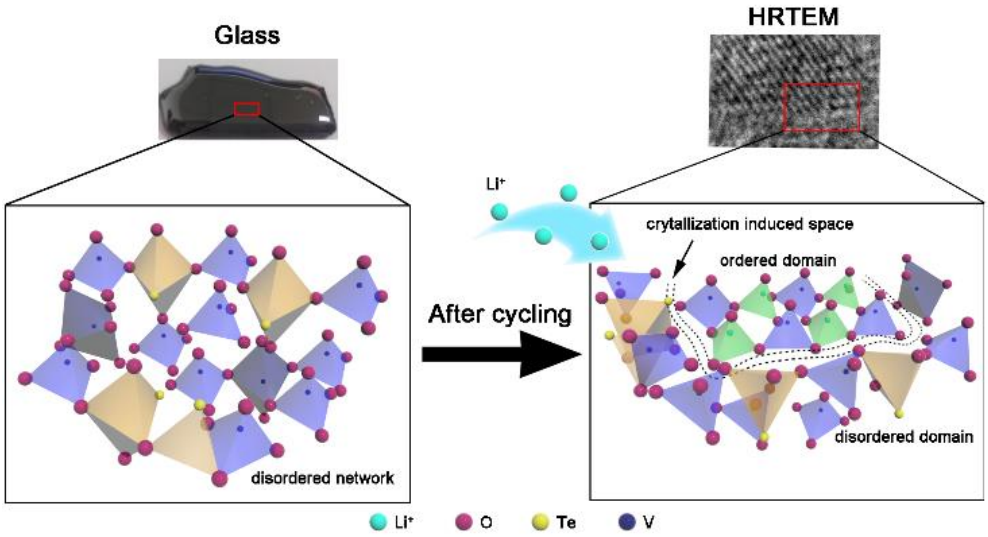

Fig. 5. A schematic representation for the structural evolution of VT 60 glass anode after 5000 discharging/charging cycles.

In addition to the γ-type, Li_3VO_4 also has a low temperature phase, namely β-type, which has been extensively studied as an insertion anode for LIBs due to its large capacity and safe voltage [2,16,27,30,32,58-61]. For instance, to provide large surfaces for Li^+ flux and short Li^+ ion diffusion paths, different methods were employed to control the particle size of β-Li_3VO_4 electrodes [29,30]. Since the β-Li_3VO_4 is an electrical insulator, fabricating a composite by coating the particles with carbon to increase the electronic conductivity of the anode material is another effective way to improve the battery performance [59,60].

Compared to the β-type, γ-Li_3VO_4 is a metastable phase and enables lithium ions

diffuse more easily, and therefore it is one of the promising phases for fabricating superior electrode materials [62,63]. However, γ-Li_3VO_4 is only stable at high temperature and would spontaneously convert into the low temperature β phase during cooling. In other words, it is hard to generate the γ-Li_3VO_4 phase. This is also why most of the studies focused on the β-Li_3VO_4 phase as anode material. Remarkably, the γ-Li_3VO_4 nanocrystals were obtained from the VT60 glass anodes at room temperature through disorder/order engineering, i.e., upon multiple discharging/charging cycling of the glass phase, as shown in Figs. 2b and 3. The potential energy of γ-Li_3VO_4 is lower than that of its parent glass, but higher than that of β-Li_3VO_4. Accordingly, the γ-form has more open structure than the β-form since the former inherits the heterogeneous structure of its supercooled liquid.

Based on the above analysis, the high-rate capability and excellent long-life performance of VT60 glass must be ascribed to the reconstructed architecture, in which the γ-Li_3VO_4 nanocrystals are embedded in the semiconducting glass matrix. To be specific, the enhanced ionic conductivity is the first indicator of the improvement of the electrochemical performances of Li_3VO_4 anode [29]. The formed γ-Li_3VO_4 itself has higher ionic conductivity [62,63] than that of the widely studied β form. Moreover, the γ-Li_3VO_4 nanocrystals can greatly shorten the Li^+ diffusion path, resulting in higher ionic conductivity of the anode materials. The enhanced cycling stability is the second indicator of the improved electrochemical performances. The open network in the glass matrix can buffer the crystal structure variations [18,27] induced by repetitive Li^+ intercalation/de-intercalation to avoid the stress-induced microcracks [64]. In addition, the γ-Li_3VO_4 nanocrystals and the induced excessive space or channels (Fig. 5) can play roles in suppressing the propagation of the micro-cracks to sustain 5000 discharging/charging cycles and even beyond. Consequently, both the ion transfer and the cycling stability of the glass anode are greatly enhanced. In contrast to the enhancement of the anode performance by disorder-order transition shown in this work, it was recently found that the order-disorder transition could also facility the lithium diffusion in the Fe-doped

$LiMnPO_4$ cathode Li-ion batteries owing to the higher octahedral distortion of (Mn, Fe)O_6 caused by introduction of Fe [65]. In addition, the order-disorder transition was found to be an effective way in improving sodium storage performance and excellent cycling stability of $NaFePO_4$ cathode in sodium ion batteries [66].

Conclusions

We have clarified the origin of both the discharging/charging induced nanocrystal formation in VT60 glass anode and the resulting enhancement of the Li-ion battery performances. The VT60 glass displays superior reversible capacity and outstanding long discharging/charging cycling stability. The remarkable electrochemical performances have been attributed to: 1) the intrinsic rapid ionic conductivity of γ-Li_3VO_4 nanocrystals; 2) the shortened Li^+ diffusion pathway due to the formation of the nano-crystals; 3) the electronic conductivity brought by the glass phase; and 4) the robust structure of the anode.

We have proposed the microscopic scenario of the charging induced nucleation. The Li ions 'hit' the higher energy domains of structural network of VT60 glass during discharging/charging, and some of those Li ions join the network rearrangement, during which the potential energy is lowered through nanocrystal formation. Such kind of nanocrystal formation is associated with its low glass stability against crystallization and high degree of structural heterogeneity of the VT glasses. In other words, the repetitive insertion/extraction of Li^+ ions weakens the high-energy domains of the structural network and thereby increases the probability of those domains to be rearranged towards the ordered pattern with lower potential energy, leading to formation of the γ-Li_3VO_4 nanocrystals in the glass matrix.

Acknowledgments

This work was financially supported by National Natural Science Foundation of China (51402156) and Shandong Provincial Natural Science Foundation (ZR2014EMQ003, ZR2018QB003).

References:

[1] H. D. Yoo, E. Markevich, G. Salitra, D. Sharon, D. Aurbach, Mater. Today 17 (2014)110-121.

[2] C. Y. Liao, Q. Zhang, T. Y. Zhai, H. Q. Li, H. S. Zhou, Energy Storage Mater. 7 (2017) 17-31.

[3] Z. L. Jian, M. B. Zheng, Y. L. Liang, X. X. Zhang, S. Gheytani, Y. C. Lan, Y. Shi, Y. Yao, Chem. Commun. 51 (2015) 229-231.

[4] Q. T. Xu, J. C. Li, H. G. Xue, S. P. Guo, J. Power Sources 379 (2018) 41-52.

[5] Z. H. Ma, Y. S. Wang, C. W. Sun, J. A. Alonso, M. T. Fernandez-Diaz, L. Q. Chen, Scientific Reports 4 (2014) 7231.

[6] E. Yoo, J. Kim, E. Hosono, H. Zhou, T. Kudo, I. Honma, Nano Lett. 8 (2008) 2277.

[7] F. Ji, Y. L. Li, J. M. Feng, D. Su, Y. Y. Wen, Y. Feng, F. Hou, J. Mater. Chem. 19 (2009) 9063-9067.

[8] M. Liang, L. Zhi, J. Mater. Chem. 19 (2009) 5871-5878.

[9] C. M. Park, J. H. Kim, H. Kim, H. J. Sohn, Chem. Soc. Rev. 39 (2010) 3115-3141.

[10] U. Kasavajjula, C. S. Wang, A. J. Appleby, J. Power Sources 163 (2007)1003-1039.

[11] X. H. Liu, L. Zhong, S. Huang, S. X. Mao, T. Zhu, J. Y. Huang, ACS Nano 6 (2012) 1522-1531.

[12] M. Winter, J. O. Besenhard, M. E. Spahr, P. Novak, Adv. Mater. 10 (1998) 725-763.

[13] M. Zukalova, M. Fabian, M. Klusackova, M. Klementova, B. P. Laskova, Z. Dankova, M. Senna, L. Kavan, Electrochim. Acta 265 (2018) 480-487.

[14] S. Zhu, J. Li, X. Deng, C. He, E. Liu, F. He, C. Shi, N. Zhao, Adv. Funct. Mater. 27 (2017) 1605017.

[15] A. A. AbdelHamid, Y. Yu, J. Yang, J. Y. Ying, Adv. Mater. 29 (2017) 1701427.

[16] L. Chen, X. Jiang, N. Wang, J. Yue, Y. Qian, J. Yang, Adv. Sci. 2 (2015) 1500090.

[17] B. A. Boukamp, G. C. Lesh, R. A. Huggins, J. Electrochem. Soc. 128 (1981) 725-729.

[18] Y. F. Zhang, P. X. Wang, T. Zheng, D. M. Li, G. D. Li, Y. Z. Yue, Nano Energy 49 (2018) 596-602.

[19] C. Gejke, L. Beorjesson, K. Edstreom, Electrochem. Commun. 5 (2003) 27-31.

[20] H. Yamauchi, G. Park, T. Nagakane, T. Honma, T. Komatsu, T. Sakai, A. Sakamoto, J. Electrochem. Soc. 160 (2013) A1725-A1730.

[21] Y. Idota, T. Kubota, A. Matsufuji, Y. Maekawa, T. Miyasaka, Science 276 (1997) 1395-1397.

[22] H. Morimoto, M. Tatsumisago, T. Minami, Electrochemical and Solid-State Letters 4 (2001) A16-A18.

[23] J. H. Ku, J. H. Ryu, S. H. Kim, O. H. Han, S. M. Oh, Adv. Funct. Mater. 22 (2012) 3658-3664.

[24] R. N. Sinclair, A. C. Wright, B. Bachra, Y. B. Dimitriev, V. V. Dimitrov, M. G. Arnaudov, J. Non-Cryst. Solids 232-234 (1998) 38-43.

[25] H. Mori, J. Non-Cryst. Solids 463 (2017) 163-168.

[26] W. He, X. D. Zhang, C. Jin, Y. Y. Wang, S. Mossin, Y. Z. Yue, J. Power Sources 342 (2017) 717-725.

[27] Z. Liang, Y. Zhao, L.Ouyang, Y. Dong, Q. Kuang, X. Lin, X. Liu, D. Yan, J. Power Sources 252 (2014) 244-247.

[28] H. L. Yu, C. Ma, B. H. Ge, Y. J. Chen, Z. Xu, C. L. Zhu, C. Y. Li, Q. Y. Ouyang, P. Gao, J. Q. Li, C. W. Sun, L. H. Qi, Y. M. Wang, F. H Li, Chem. Eur. J. 19 (2013) 5818-5823.

[29] S. Ni, X. Lv, J. Ma, X. Yang, L. Zhang, J. Power Sources 248 (2014) 122-129.

[30] W. T. Kim, Y. U. Jeong, Y. J. Lee, Y. J. Kim, J. H. Song, J. Power Sources 244 (2013) 557-560.

[31] Y. Zhang, J. Y. Lai, Y. D. Gong, Y. M. Hu, J. Liu, C. W. Sun, Z. L. Wang, ACS Appl. Mater. Inter. 8 (2016) 34309-34316.

[32] N. Liu, Z. Lu, J. Zhao, M. T. McDowell, H. W. Lee, W. Zhao, Y. Cui, Nat.

Nanotechnol. 9 (2014) 187-192.

[33] I. Gutzow, Contemp. Phys. 21 (1980) 121-137.

[34] K. Matusita, T. Komatsu, R. Yokota, J. Mater. Sci. 19 (1984) 291-296.

[35] Y. F. Zhang, G. Yang, and Y. Z. Yue, J. Am. Ceram. Soc. 96 (2013) 3035-3037.

[36] J. B. Lee, J. Moon, O. B. Chae, J. G. Lee, J. H. Ryu, M. Cho, K. Cho, S. M. Oh, Chem. Mater. 28 (2016) 5314-5320.

[37] X. M. Jian, H. Q. Wenren, S. Huang, S. J. Shi, X. L. Wang, C. D. Gu, J. P. Tu, J. Power Sources, 246 (2014) 417-422.

[38] G. Silversmit, D. Depla, H. Poelman, G. B. Marin, R. D. Gryse, J. Electron. Spectrosc. Relat. Phenom. 135 (2004) 167-175.

[39] Y. Z. Yue, Q. J. Zheng, Int. J. Appl. Glass Sci. (2016) 1-11.

[40] A. A. Cabral Jr., C. Fredericci, E. D. Zanotto, J. Non-Cryst. Solids 219 (1997) 182-186.

[41] M. L. F. Nascimento, L. A. Souza, E. B. Ferreira, E. D. Zanotto, J. Non-Cryst. Solids 351 (2005) 3296-3308.

[42] A. Hruby, Czech. J. Phys. B 22 (1972) 1187-1193.

[43] M. Moesgaard, Y. Z. Yue, J. Non-Cryst. Solids, 355 (2009) 867-873.

[44] Y. Z. Yue, J. Non-Cryst. Solids 345&346 (2004) 523-527.

[45] F. H.Stillinger, T. A.Weber, Phys. Rev. A. 28 (1983) 2408.

[46] G. S. Matharoo, M. S. G. Razul, P. H. Poole, Phys. Rev. E 74 (2006) 050502.

[47] H. Sillescu, J. Non-Cryst. Solids 243 (1999) 81-108.

[48] L. S. Huo, J. F. Zeng, W. H. Wang, C. T. Liu, Y. Yang, Acta Mater. 61 (2013) 4329-4338.

[49] W. D. Li, H. Bei, Y. Tong, W. Dmowski, Y. F. Gao, Appl. Phys. Lett. 103 (2013) 171910.

[50] Y. Z. Yue, C. A. Angell, Nature, 427 (2004) 717-720.

[51] Y. F. Zhang, L. N. Hu, S. J. Liu, C. F. Zhu, Y. Z. Yue, J. Non-Cryst. Solids 381 (2013) 23-28.

[52] J. Kjeldsen, A. C. M. Rodrigues, S. Mossin, Y. Z. Yue, J. Phys. Chem. B 118

(2014) 14942-14948.

[53] L. N. Hu, Y. Z. Yue, J. Phys. Chem. B 112 (2008) 9053-9057.

[54] S. J. Liu, Y. F. Zhang, Y. Z. Yue, Phys. Chem. Glasses: Eur. J. Glass Sci. Technol. B, 52 (2011) 231-235.

[55] T. Kawasaki, H. Tanaka, J. Phys.: Condens. Matter, 22 (2010) 232102.

[56] H. Shintani, H. Tanaka, Nat. Phys. 2 (2006) 200-206.

[57] Y. Sun, H. Xi, S. Chen, M. D. Ediger, L. Yu, J. Phys. Chem. B 112 (2008) 5594-5601.

[58] H. Q. Li, X. Z. Liu, T. Y. Zhai, D. Li, H. S. Zhou, Adv. Energy Mater. 3 (2013) 428-432.

[59] Y. Shi, J. Z. Wang, S. L. Chou, D. Wexler, H. J. Li, K. Ozawa, H. K. Liu, Y. P. Wu, Nano Lett. 13 (2013) 4715-4720.

[60] Z. L. Jian, M. B. Zheng, Y. L. Liang, X. X. Zhang, S. Gheytani, Y. C. Lan, Y. Shi, Y. Yao, Chem. Commun. 51 (2015) 229-231.

[61] R. D. Shannon, C. Calvo, J. Solid State Chem. 6 (1973) 538-549.

[62] A. K. I. Shitz, V. V. Kireev, O. K. Melnikov, L. N. Demianets, Crystallogr. Rep. 46 (2001) 864-867. Translated from Kristallografiya, 46 (2001) 938-941.

[63] C. Liao, Y. Wen, Z. Xia, R. Qin, X. Liu, Y. Yu, B. Shan, T. Zhai, H. Li, Adv. Energy Mater. 8 (2017) 1701621.

[64] S. Q. Li, Q. Wu, D. Zhang, Z. S. Liu, Yi He, Z. L. Wang, C. W. Sun, Nano Energy 56 (2019) 555-562.

[65] S. Q. Li, X. Y. Meng, Q. Yi, J. A. Alonso, M. T. Fernandez-Diaz, C. W. Sun, Z. L. Wang, Nano Energy 52 (2018) 510-516.

[66] F. Y. Xiong, Q. Y. An, Y. Zhao, L. X. Xia, L. Q. Mai, H. Z. Tao, Y. Z. Yue, Nano Energy (under review).

Highlights

- We clarified the Li-insertion induced nucleation in glass anode of Li-ion batteries.
- Ionic conductivity and cycling stability were enhanced by nanocrystal formation.
- The nanocrystals in 40TeO2-60V2O5 glass were identified to be γ-Li3VO4 phase.
- γ-Li3VO4 is a metastable phase benefiting the enhancement of Li-ion conductivity.
- We explained the origin of the remarkable electrochemical performances.